AAS 15-383

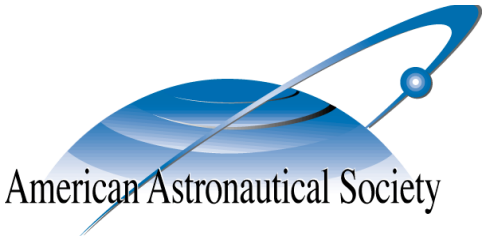

American Institute of
Aeronautics and Astronautics

TOUCHLESS ELECTROSTATIC DETUMBLING WHILE TUGGING LARGE AXI-SYMMETRIC GEO DEBRIS

Trevor Bennett and Hanspeter Schaub

AAS/AIAA Spaceflight Mechanics Meeting

Williamsburg, Virginia **January 11–15, 2015**

AAS Publications Office, P.O. Box 28130, San Diego, CA 92198

(Preprint) AAS 15-383

TOUCHLESS ELECTROSTATIC DETUMBLING WHILE TUGGING LARGE AXI-SYMMETRIC GEO DEBRIS

Trevor Bennett* **and Hanspeter Schaub†**

Touchless detumbling of the three-dimensional spin of axi-symmetric space debris is investigated to enable orbital servicing or active debris removal in the Geosynchronous belt. Using active charge transfer between a servicing spacecraft and debris object, control torques are created to reduce the debris spin rate prior to making any physical contact. First considered is the addition of nominal tugging and pushing of deep space 3-dimensional detumble. The proposed control provides momentum reduction and clear equilibrium surfaces. This work also extends the projection angle theory for three-dimensional tumbling motion to on-orbit relative motion. Prior work has identified the limitations of electrostatic detumble for three degree rotational freedom without relative positioning maneuvers. Using the Multi-Sphere Modeling method for electrostatic torques, servicer formation flying demonstrates improved detumble capability. The numerically simulated orbiting along-track formation provides a natural relative inertial motion that helps remove all debris angular velocity except for the spin about the symmetry axis.

INTRODUCTION

Orbital servicing is a challenging space mission concept that requires a servicing vehicle to approach and mechanically interface with a defunct satellite or satellite component.[1,2,3] If the debris is tumbling, the docking process becomes challenging or impossible and presents a significant collision risk. Advanced docking systems such as those being developed by MDA discuss a maximum tumble rate of 1 degree/second for autonomous docking.[4] Touchless methods, such as the the Electrostatic Tractor (ET), are being considered for both large GEO debris mitigation.[5,6,7] Reference 8 discusses how electrostatic torque can be controlled to apply torques on a spinning debris object without requiring physical contact as shown in Figure 1. The charging is controlled through an electron gun aimed at the debri charging the servicer positively and the debris negatively. The resulting potential difference creates the attractive force capable of detumbling the target object. Touchless electrostatic detumble of large Geosynchronous (GEO) debris objects is the focus of this paper. The applications of a touchless method may extend beyond GEO to encompass asteroid interaction or spin control.[9,10]

Electrostatic actuation of spacecraft has been explored since the 1960s. Reference 11 highlights the Geosynchronous Orbit environment as a candidate region where the space plasma conditions enable Debye lengths on the order of 100's of meters. As a result, electrostatic control requires only Watt-levels of power requirements. The fuel efficiency in implementing electrostatic actuation is counterbalanced by increased complexity and highly-coupled nonlinear differential equations.[12]

*Graduate Research Assistant, Aerospace Engineering Sciences, University of Colorado.
†Professor, Department of Aerospace Engineering Sciences, University of Colorado, 431 UCB, Colorado Center for Astrodynamics Research, Boulder, CO 80309-0431

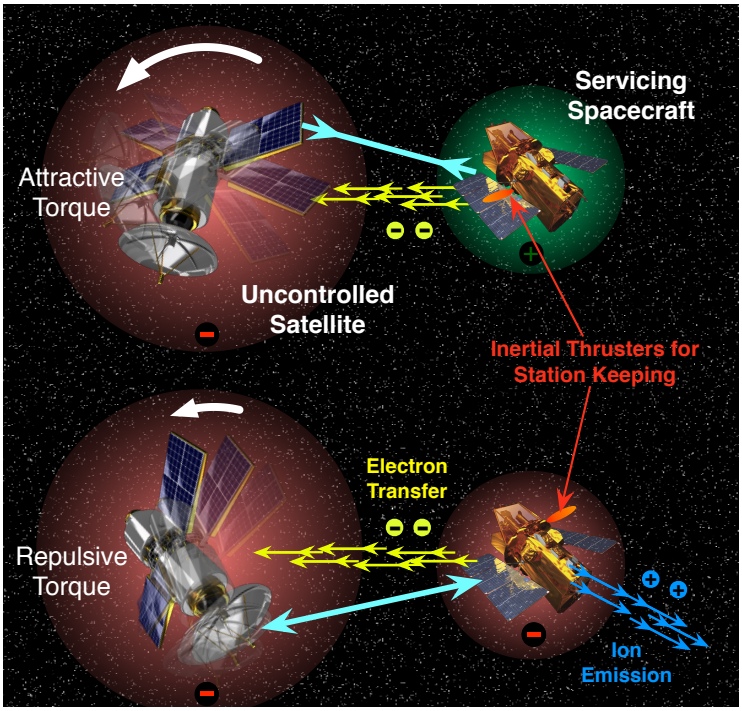

Figure 1. Electrostatic Detumbling Concept Illustration.

Overcoming the control and modeling complexity enables servicing spacecraft to impart relative potentials on itself and either another controlled spacecraft or an uncooperative body. Non-cooperative electrostatic control sees application in orbital space debris mitigation, orbital servicing, and detumble for rates exceeding the capabilities of current docking or grappling techniques.

The feasibility of electrostatic control and actuation in space has been explored by several authors for a diverse range of applications from formation flying to deployable structures.[13,14,15,16,17,18,19] Electrostatic interaction between two spacecraft in a vacuum is accurately determined using finite element methods; however, these methods are computationally expensive. Stevenson and Schaub introduced a new method called the Multi-Sphere Method (MSM)[12,20] that approximates the electrostatic interaction between spacecraft with orders of magnitude less computational time, enabling attitude simulations and control developments. The multi-sphere method, summarized in detail during the following sections, partitions the spacecraft volume into a series electrostatic conducting spheres held at a common spacecraft potential. Using the recently developed MSM technique, Reference 8 studies the charged relative one-dimensional rotational dynamics of a non-cooperative cylinder and a spherical charge-controlled spacecraft with experimental validation.[21]

Reference 22 generalized the one dimensional detumble representation to three dimensional general tumble. Identified were specific debris attitudes where the servicer spacecraft has no control authority on the debris tumble. The fixed servicing spacecraft relative position inhibits the production of differential using the 3-sphere MSM model employed such that no differential torques are produced. Desired are servicer relative motions that prevent loss of control authority. The orbital motion, shown in Figure 2 motivates study into servicer relative orbits influenced by electrostatic detumble. The relative position shown at the bottom of Figure 2 shows where the electrostatic force has a greater effect on the nearest part of the debris object and therefore induces a differential torque.

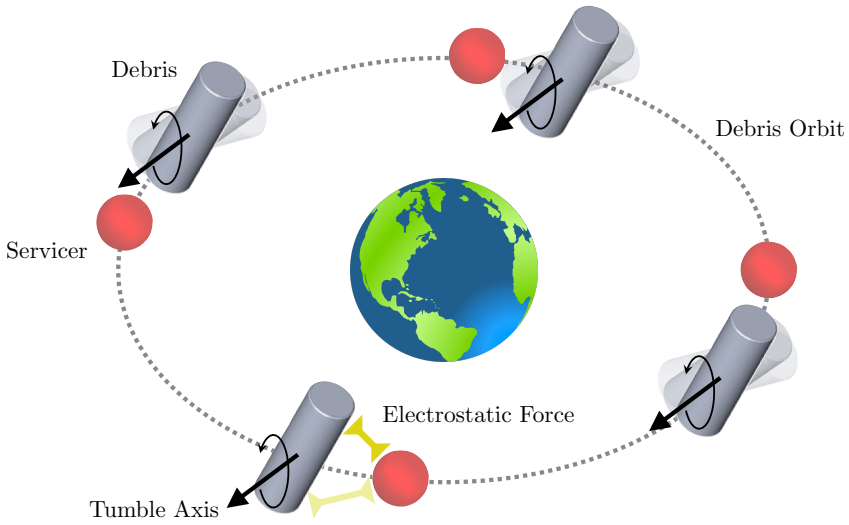

Figure 2. Relative motion of servicer spacecraft around tumbling debris object.

In the relative position shown on either side of Figure 2 shows where minimal or zero differential torque is generated. Earlier work explores Coulomb formation flying and tug trajectories.[23,24] In contrast, this work addresses relative motion applied to detumble of the debris object. This work expands the prior analysis to consider natural relative orbital motion and the stability of nominal attractive or repulsive electrostatic tractor present while the detumble is performed. Several approaches using Coulomb and Lorentz force have been studied to utilize the electrostatic effects for satellite formation flying.[25,26,27] However, this work addresses the advantages of relative orbits on detumble performance.

Upper stage rocket bodies form a large component of GEO debris, justifying the assumption of a cylindrical debris shape for the scope of this paper. Of interest is how torque equilibriums impact the convergence of the general tumbling scenario, the stability of such equilibria, and the development of a general detumble and relative motion control algorithm. The following sections detail the Multi-Sphere Method and the previously developed attitude description. The paper concludes with the work in progress.

MULTI-SPHERE METHOD

The Multi-Sphere Method (MSM) represents the complete spacecraft electrostatic charging model as a collection of spherical conductors carefully dispersed through the body.[12] The cylinder configuration representative of the above mentioned rocket bodies and defunct spacecraft is detailed in Figure 3. The 3-sphere MSM approximation provides sufficient force and torque accuracy for the separation distances considered.[20]

The modeled configuration parameters are the separation distance d, the cylinder rotation about the inertial z axis θ, the pitch angle defined from the inertial x-y plane ψ, and the control voltages ϕ_1 and ϕ_2. The inertial coordinate system is fixed to the controlled spherical spacecraft with the z

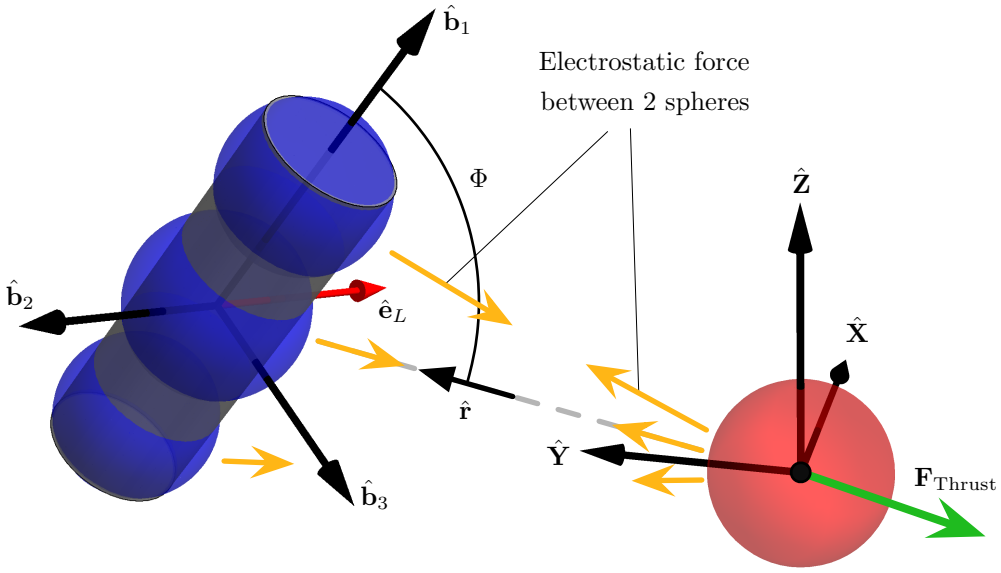

Figure 3. 3 sphere MSM cylinder and spherical spacecraft configuration.

axis pointed up, the y axis pointed along the relative distance vector, and the x axis completing a right-handed system. The cylinder has body fixed aircraft-type coordinates with $\hat{b}_1$ through the long axis, $\hat{b}_3$ pointed down , and $\hat{b}_2$ for a right handed system. This positive cylinder pitch of is described as a positive $\hat{b}_2$ rotation.

The electrostatic forces are determined by the charges residing on each sphere. These result from the prescribed electric potentials, according to the self and mutual capacitance relationships in Equation 1, where $k_c = 8.99 \times 10^9 Nm^2/C^2$ and q_i is the charge of each sphere.[28,29]

$$\phi_i = k_c \frac{q_i}{R_i} + \sum_{j=1, j\neq i}^{m} k_c \frac{q_j}{r_{i,j}} \tag{1}$$

These relations can be represented in matrix form

$$\begin{bmatrix} \phi_1 \\ \phi_2 \\ \phi_3 \\ \phi_4 \end{bmatrix} = k_c \begin{bmatrix} 1/R_1 & 1/r_a & 1/r_b & 1/r_c \\ 1/r_a & 1/R_{2,a} & 1/l & 1/2l \\ 1/r_b & 1/l & 1/R_{2,b} & 1/l \\ 1/r_c & 1/2l & 1/l & 1/R_{2,c} \end{bmatrix} \begin{bmatrix} q_1 \\ q_a \\ q_b \\ q_c \end{bmatrix} \tag{2}$$

Inverting the matrix multiplying the charge at a given instant in time produces the forces and torques given by the summations

$$\boldsymbol{F}_2 = k_c q_1 \sum_{i=a}^{c} \frac{q_i}{r_i^3} \boldsymbol{r}_i \tag{3}$$

$$\boldsymbol{L}_2 = k_c q_1 \sum_{i=a}^{c} \frac{q_i}{r_i^3} \boldsymbol{r}_{2,i} \times \boldsymbol{r}_i \tag{4}$$

The servicing sphere and debris cylinder remain at a constant separation distance requiring a thrusting force to counter-balance the net attractive or repulsive electrostatic forces on each spacecraft. The control development assumes the necessary thrust force is present and the relative motion of the spacecraft is captured.

DEEP SPACE DETUMBLE WITH NOMINAL TUGGING AND PUSHING

The following develops the deep space detumble attitude dynamics and stability arguments when a nominal attractive or repulsive potential is prescribed. The nonimal potential serves as a tug or push to translate the entire system.

Debris Attitude Description

The detumble control, developed previously, relies on the simplified dynamics achieved for the given spherical servicer craft and cylindrical debris object. The axisymmetric debris object with internal MSM spheres does not have a torque component about the cylinder slender axis, the $\hat{\boldsymbol{b}}_1$ axis.[22] Therefore the torque axis and projection angle about the torque axis are defined.

$$\hat{\boldsymbol{e}}_L = \hat{\boldsymbol{b}}_1 \times -\hat{\boldsymbol{r}} \tag{5}$$

$$\Phi = \arccos\left(\hat{\boldsymbol{b}}_1 \cdot (-\hat{\boldsymbol{r}})\right) \tag{6}$$

where $\hat{\boldsymbol{r}}$ is the unit direction from the servicer spacecraft mass center to the tumbling body mass center, or the direction of the relative position vector. It was shown in Reference 22 that through the use of this projection angle of a cylinder slender axis onto the relative position vector, that the three dimensional rotation equations of motion reduce to scalar equations of the for in Eq (7). Consistent with the assumption of an axi-symmetric geometry, there exists no control authority in the slender axis, $\hat{\boldsymbol{b}}_1$, scalar equation because no cross coupling is present. The presented form is accurate for an inertially fixed relative position vector.

$$I_a \dot{\omega}_1 = 0 \tag{7a}$$

$$I_t \dot{\eta} - I_a \omega_1 \dot{\Phi} \sin\Phi = 0 \tag{7b}$$

$$I_t \left(\ddot{\Phi} \sin\Phi - \eta^2 \frac{\cos\Phi}{\sin^2\Phi} \right) + I_a \omega_1 \eta = L \tag{7c}$$

where I_a is the axial moment of inertia, I_t is the transverse moment of inertia, and the pseudo angular velocities are defined by

$$\eta \equiv -\omega_2(\hat{\boldsymbol{r}} \cdot \hat{\boldsymbol{b}}_2) - \omega_3(\hat{\boldsymbol{r}} \cdot \hat{\boldsymbol{b}}_3) \tag{8a}$$

$$\dot{\Phi} \sin\Phi = -\omega_2(\hat{\boldsymbol{r}} \cdot \hat{\boldsymbol{b}}_3) + \omega_3(\hat{\boldsymbol{r}} \cdot \hat{\boldsymbol{b}}_2) \tag{8b}$$

$$\boldsymbol{L} = -L\hat{\boldsymbol{e}}_L = -f(\phi)\sin(2\Phi)\,\hat{\boldsymbol{e}}_L \tag{8c}$$

Considered is a control law that successfully drives the projection angle rate to zero. Without loss of generality, the non-cooperative cylinder is assumed to have the same potential magnitude as the servicer, that is $\phi_2 = |\phi_1|$, and is assumed to be always positive.[8] Thus, the voltage dependency function is set to:[8]

$$f(\phi) = \phi|\phi| \tag{9}$$

Thus lending the control previously studied by Reference 22 is the stability of the 3-dimensional projection angle formulation expansion first proposed by Reference 8:

$$f(\phi_1) = -\text{sgn}\left(\sum_{m=1}^{n} g_m(\Phi)\right) f(\phi_{\max}) \frac{\arctan(\alpha\dot{\Phi})}{\pi/2} \tag{10}$$

where $\alpha > 0$ is a constant feedback gain and $f(\phi_{\max})$ is the maximum feasible potential available. The control law as shown in Eq. (10) provides proven asymptotic reduction of the projection angle rate.[22] However, the presented form does not provide nominal pushing or pulling authority nor stability proof. The following section details the inclusion of nominal pushing and pulling into the control formulation and provides a Lyapunov proof of stability.

Detumble Control with Nominal Tugging and Pushing

Variation to the 3-dimensional detumble previously discussed, the circumstance where the servicing spacecraft is imparting a nominal push or pull on the debris object may also be desired. The electrostatic push or pull is obtained by a non-zero nominal control potential with discussion constrained to an inertially fixed relative position vector. Consider the projection angle expansion of the non-zero nominal potential form first proposed by Reference 8

$$V(\Phi, \dot{\Phi}) = \frac{1}{2}\boldsymbol{\omega}^T I \boldsymbol{\omega} + \beta \int_0^{\Phi} g_m(x)\mathrm{d}x \tag{11}$$

where $g(x)$ is

$$g_m(\Phi) = \sum_{m=1}^{n} \gamma_m \sin(2\Phi) \tag{12}$$

with $\alpha > 0$ being a constant feedback gain and the function h is constrained such that:[8]

$$h(x)x > 0 \quad \text{if } x \neq 0 \tag{13}$$

For this study, the following function h is proposed:

$$h(\alpha\dot{\Phi}) = f(\phi_{\max}) \frac{\arctan(\alpha\dot{\Phi})}{\pi/2} \tag{14}$$

The Lyapunov function in Eq. (11) is positive definite when restrictions are placed on γ_m based on the projection angle function $g(x)$.

The assurance of a positive definite Lyapunov function enables the time derivative of Eq. (11) to be taken.

$$\dot{V}(\Phi, \dot{\Phi}) = \boldsymbol{\omega}^T \boldsymbol{L} + \beta g_m(\Phi)\dot{\Phi} \tag{15}$$

Including the detumble control torque into the Lyapunov derivative and collecting terms, the simplified form of Eq. (15) becomes Eq. (16).

$$\dot{V}(\Phi, \dot{\Phi}) = \left[f(\phi_1)\sin\Phi + \beta\right] g_m(\Phi)\dot{\Phi} \tag{16}$$

The desired form of the control provides reduction of the projection angle rate $\dot{\Phi}$ to zero prescribing that the bracketed terms in Eq. (16) equate to the desired controller in the stable control in Eq. (10) the expression in Eq. (17).

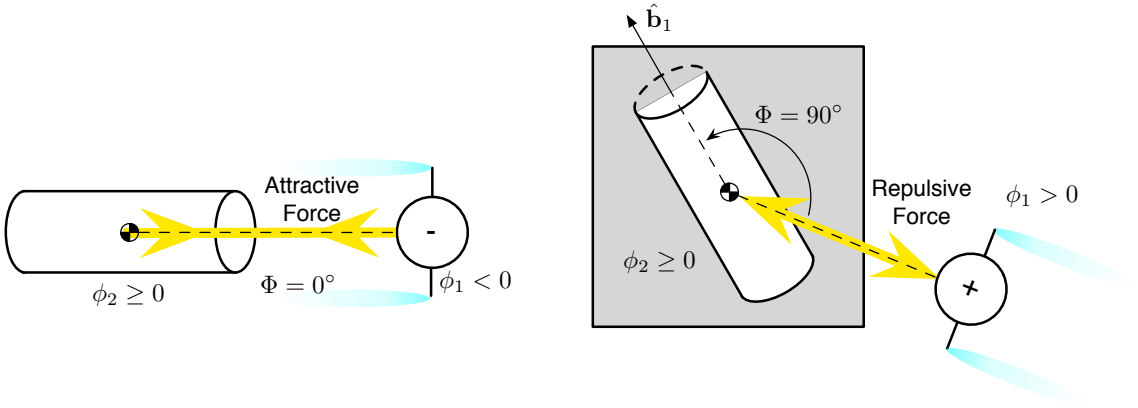

(a) Nominal Tugging

(b) Nominal Pushing

Figure 4. Equilibrium attitudes for nominal tugging and pushing potentials in deep space.

$$f(\phi_1) = -\frac{\beta}{\sin(\Phi)} - \text{sgn}\left(g_m(\Phi)\right) h(\alpha\dot{\Phi}) \tag{17}$$

The leading term in Eq. (17) represents the nominal potential prescribed for electrostatic pushing and pulling. Therefore the β feed-forward gain is defined as

$$\beta = -f(\phi_{\text{nom}}) \sin(\Phi) \tag{18}$$

Substituting the resulting new potential of Eq. (17) with defined β into the expression in Eq. (16) provides the final form for the Lyapunov derivative.

$$\dot{V}(\Phi, \dot{\Phi}) = \left[-\beta - \text{sgn}\left(g_m(\Phi)\right) h(\alpha\dot{\Phi}) \sin(\Phi) + \beta\right] g_m(\Phi)\dot{\Phi} \tag{19a}$$

$$= -\text{sgn}\left(g_m(\Phi)\right) g_m(\Phi) \sin(\Phi) h(\alpha\dot{\Phi})\dot{\Phi} \tag{19b}$$

which is shown to be negative semi-definite by Reference 22 around $\Phi = 0$ and provides asymptotic stability with additional invariant set arguments. Given a nominal pushing or pulling electrostatic potential, the control form presented provides asymptotic convergence to a nulled projection angle rate. Using a projection angle form, the nominal equilibrium projection angles from the analysis in Reference 8 apply. Inclusion of a attractive nominal potential, the cylinder rests at a projection angle of zero. Inclusion of a repulsive nominal potential rests the cylinder at a projection angle of $90°$. However, given that the projection angle describes a 3-dimensional attitude the interpretation of the equilibrium angle is different than previous studies. A projection angle of zero, that of the nominal tugging case, is unambiguous and refers to a perfect alignment between the slender axis of the cylinder and the relative position vector. A projection angle of $\Phi = 90°$ provides an infinite set of attitudes as the projection angle only defines an admissible plane for the slender axis to reside within. Therefore, any combination of body attitudes and angular rates that restricts the slender axis to the plane for all time is admissible as an equilibrium state with nominal repulsive force. This 3-dimensional definition of the projection angle fully encapsulates previous results and is applicable to more a general tumble of a debris cylinder.

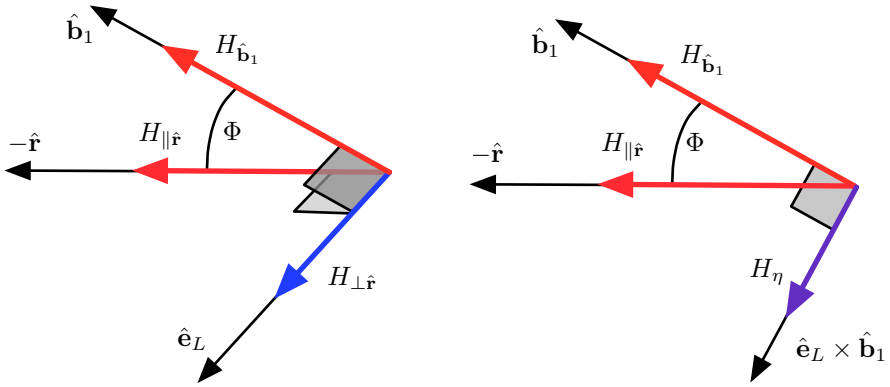

(a) 3D momentum vector components (b) Planar momentum vector components

Figure 5. Component breakdown of momentum. Colored to represent the ability for detumble influence.

ON ORBIT ELECTROSTATIC DETUMBLE WITH ZERO NOMINAL POTENTIAL

Of great interest is the control law detumble performance while the servicer and debris are in orbit. Prior analysis has only considered the detumble performance in deep space where the relative position vector remains stagnant as seen by the inertial frame.[8,22] The following describes the on orbit momentum decrease with the control law proposed above to discuss final attitudes of the servicer-debris system. The momentum decrease discussion is independent of orbit type. The numerical simulation applies the derived concepts to a lead-follower GEO circular orbit.

Momentum Dumping on Orbit

To stably remove angular momentum from the on orbit debris object, the following Lyapunov function provides conditions on the implemented controller.

$$V = \frac{1}{2}\boldsymbol{\omega}^T I \boldsymbol{\omega} \tag{20}$$

and derivative

$$\dot{V} = \boldsymbol{\omega}^T \boldsymbol{L} \tag{21}$$

where the electrostatic torque is always about the $\hat{e}_L$ vector such that

$$\dot{V} = -L(\boldsymbol{\omega} \cdot \hat{\boldsymbol{e}}_L) \tag{22}$$

Observing Eq. (22) the control design emerges in the prescription of the torque magnitude L. Therefore, for an implemented control to monotonically reduce the angular velocity and thereby the angular momentum, the sign of L is selected such that Eq. (22) is always negative semi-definite. The proposed controller in Eq (10) satisfies this sign requirement and therefore monotonically reduces the angular velocity.

Confidence in a stable decrease in angular momentum enables further study into the magnitude of angular momentum dumping. The angular momentum vector components can be expressed along the $\mathcal{E}$-frame and relative position vector with the decomposition graphically represented in Figure 5. Recall that angular momentum aligned with the relative position vector $H_{\|r}$ cannot be removed in

the instantaneous configuration. Using Figure 5(b) and assuming the relative position vector is fixed inertially, a nonzero $H_{\|r}$ may exist producing a body cone where $\hat{\boldsymbol{b}}_1$ sweeps around $\hat{\boldsymbol{r}}$ requiring η to also be nonzero. In such an instance would result in an incomplete reduction in angular momentum with a body cone determined by the relative magnitudes of ω_1 and η.[22]

Alternatively, if the relative position vector $\hat{\boldsymbol{r}}$ changes inertially, then the momentum decompositions shown in Figure 5 present an instantaneous snapshot. The magnitude of $H_{\|r}$ is therefore subject to the dynamics of $\hat{\boldsymbol{r}}$ suggesting that reconfiguration may remove greater angular momentum. Recall that the electrostatic torque is only produced around the $\hat{\boldsymbol{e}}_L$ vector defined by Eq (5). The detumble control produces a torque while the angular momentum derivative and the torque axis are aligned. That is:

$$\boldsymbol{L} = 0 \quad \text{IFF} \quad \dot{\boldsymbol{H}} \cdot \hat{\boldsymbol{e}}_L = 0 \tag{23}$$

Study of the cases where the torque does go to zero for all time reveals the steady state behavior of the detumble control. The classical Euler rotational equations are defined for an axi-symmetric body.

$$\dot{\boldsymbol{H}} = \begin{bmatrix} I_a\dot{\omega}_1 \\ I_t\dot{\omega}_2 + (I_a - I_t)\,\omega_1\omega_3 \\ I_t\dot{\omega}_3 + (I_t - I_a)\,\omega_1\omega_2 \end{bmatrix} \tag{24}$$

Taking the dot product between Eq (24) and $\hat{\boldsymbol{e}}_L$, with the definition of η defined in Eq. (8), to find where the torque is zero produces Eq. (25).

$$0 = I_t\left[\dot{\omega}_2(\hat{\boldsymbol{r}}\cdot\hat{\boldsymbol{b}}_3) - \dot{\omega}_3(\hat{\boldsymbol{r}}\cdot\hat{\boldsymbol{b}}_2)\right] + (I_a - I_t)\omega_1\eta \tag{25}$$

A steady state η can be found if Eq (25) remains true for all remaining time. The steady state η is therefore:

$$\eta_{ss} = \frac{-I_t}{\omega_1(I_a - I_t)}\left[\dot{\omega}_2(\hat{\boldsymbol{r}}\cdot\hat{\boldsymbol{b}}_3) - \dot{\omega}_3(\hat{\boldsymbol{r}}\cdot\hat{\boldsymbol{b}}_2)\right] \tag{26}$$

The leading coefficient of Eq. (26) is constant for the axi-symmetric body. Therefore, the bracketed term of Eq. (26) must remain constant at steady state thereby imposing restrictions on the final momentum of the system. Additional insight is gained through study of the modified projection angle rate equation derived from the time derivative of Eq. (6) with an non-stationary inertial relative position.

$$\dot{\Phi}\sin(\Phi) = \omega_3(\hat{\boldsymbol{r}}\cdot\hat{\boldsymbol{b}}_2) - \omega_2(\hat{\boldsymbol{r}}\cdot\hat{\boldsymbol{b}}_3) + (\hat{\boldsymbol{b}}_1\cdot\dot{\hat{\boldsymbol{r}}}) \tag{27}$$

When the controller provides no additional torque for the remainder of time, the projection angle rate must be zero. Therefore, the right hand side of Eq. (27) must be zero. Suppose the controller is successful at removing all the transverse angular velocity when $\hat{\boldsymbol{r}}$ is non-stationary. In such a case, the dot product between the slender axis and the relative position rate must be zero dictating a final projection angle of 90° for all remaining time. The implemented control uses the projection angle rate defined by Eq. (27). The performance of the control is numerically demonstrated in the following section.

Detumble Simulation in Orbital Environment

A numerical simulation is performed to validate the on-orbit detumble performance and final attitude predictions. The first simulation presents the deep space case where gravitational effects

are negligible in comparison to the electrostatic force. The second simulation presents the on-oirbit detumble with same initial relative position and tumble conditions as the deep space case. The simulations place the servicer spacecraft 12.5 meters away from a generally tumbling cylinder. The numerical simulation includes the 6-DOF motion of the debris and 3-DOF translational motion of the servicer sphere. A closed-loop servo control is used to maintain a fixed relative position between servicer and debris. A 4^{th} order Runge-Kutta integration is employed with a time step of 0.01 seconds. The servicer vehicle potential is controlled via Eq. (10), while the electrostatic force is evaluated using the full MSM model in Eqs. (2)–(4). This deep space detumble shown in Figure 6 re-creates a case from Reference 22. The cylinder is generally tumbling with a combined angular velocity of $2^\circ/\text{sec}$. The comparison of the control, projection angle, and momentum alignment are presented in Figure]reffig:sim1.

Inspection of Figure 6(a) shows the deep space projection angle collapses to a measure around 97° which is predicted by the equations of motion in Eq. (7) and the angular momentum decomposition in Figure 5. The full derivation and proof of the steady state projection angle is provided in Reference **?**. However, the deep space projection angle rate goes to zero and the implemented control turns off. The angular momentum alignment with the deep space relative position vector moves towards either 0 or 180° as seen in Figure 6(e).

Consider the same initial tumbling conditions presented above with the servicer now leading the debris object in a circular GEO orbit. Given a lead-follower relative orbit, the inertial relative position vector is no longer constant. The resulting detumble is presented in right column of Figure 6. Visible at the tail end of the control potential in Figure 6(b) is a non-zero periodic control with decreasing magnitude. The non-zero potential indicates that the implemented control can provide additional momentum dumping after the primary phase. The projection angle history in Figure 6(d) and Eq. (27) provide sufficient understanding of the supplementary momentum dumping. Inspection of Figure 6(d) shows a mean oscillation that corresponds directly to the GEO orbit period. The oscillation about this mean is reduced to near zero followed by further reduction of the mean magnitude. This reduction character is dictated by the dominant terms in Eq. (27). During the primary detumble phase, the dominant terms are the body fixed angular velocities which dwarf the $\dot{\hat{\boldsymbol{r}}}$ introduced by a GEO lead-follower relative orbit. Once the angular velocities are sufficiently reduced, the orbit motion contribution becomes dominant and the projection angle begins to collapse towards a steady-state angle. In the deep space case presented in Figure 6 the angle between the angular momentum and the relative position vector moved towards either 0° or 180°. In the on orbit case, the angular momentum vector appears to oscillate and then collapse towards an angle of 90°. This is supported by Eq. (27) where if the orbital motion remains the dominant term then the $\hat{\boldsymbol{b}}_1$ spin axis must be perpendicular to $\dot{\hat{\boldsymbol{r}}}$ for all future time. Since in a lead-follower relative orbit $\dot{\hat{\boldsymbol{r}}}$ sweeps a plane, then $\hat{\boldsymbol{b}}_1$ must reside perpendicular to the plane. If $\hat{\boldsymbol{b}}_1$ is perpendicular to the plane, which coincides with the orbit plane, then the final projection angle is $\Phi_{ss} = 90^\circ$. Such a projection angle does not appear to violate Eq. (26) and is therefore an admissible final state for the on orbit simulation.

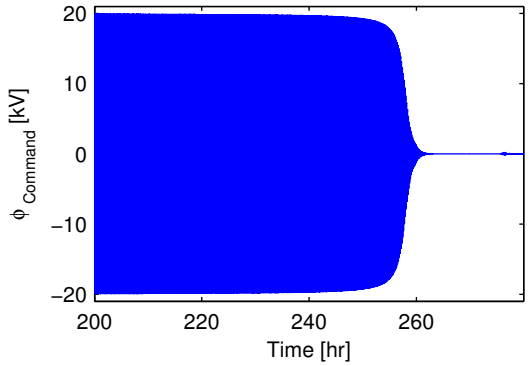

(a) Commanded Potential, Deep Space

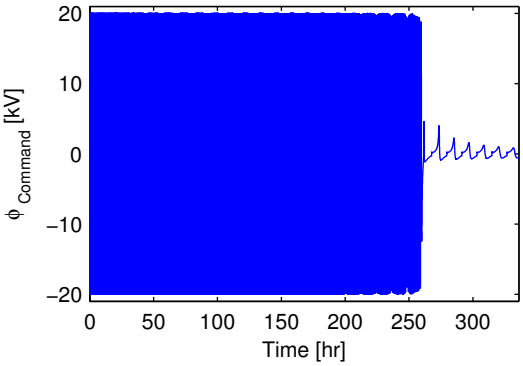

(b) Commanded Potential, On Orbit

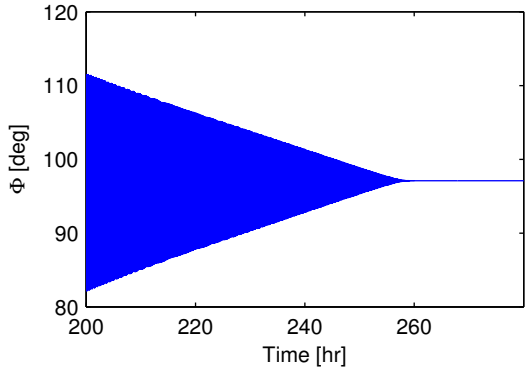

(c) Projection Angle, Deep Space

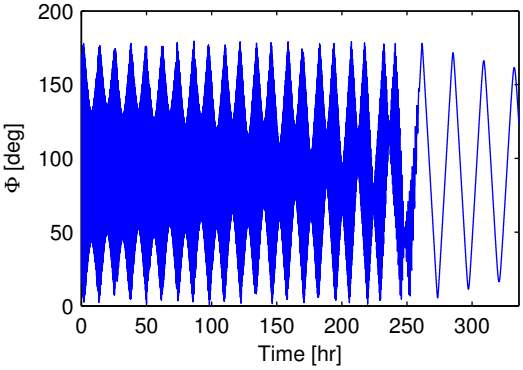

(d) Projection Angle, On Orbit

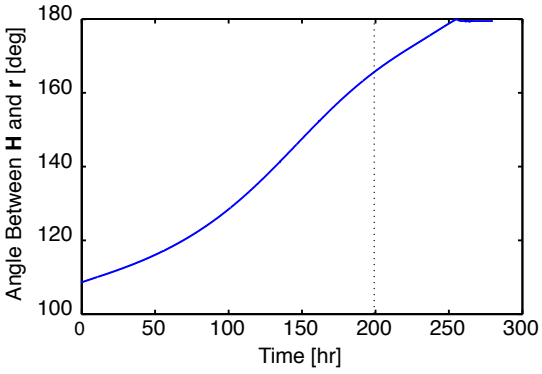

(e) Alignment of $\boldsymbol{H}$ and $\boldsymbol{r}$

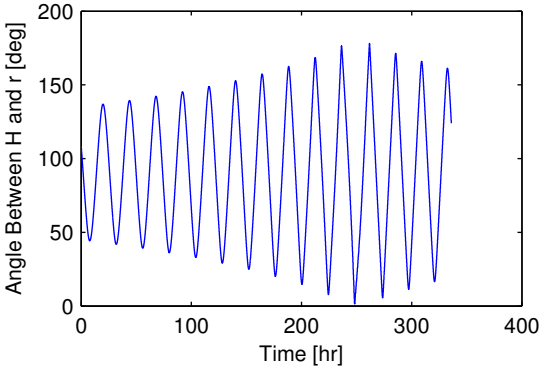

(f) Alignment, On Orbit

Figure 6. Numerical simulation with initial conditions: $\omega = [0.5, -1.374,\ 1.374]$**,** $\Phi_0 = 30°$ **comparing both deep space (left column) and on orbit (right column).**

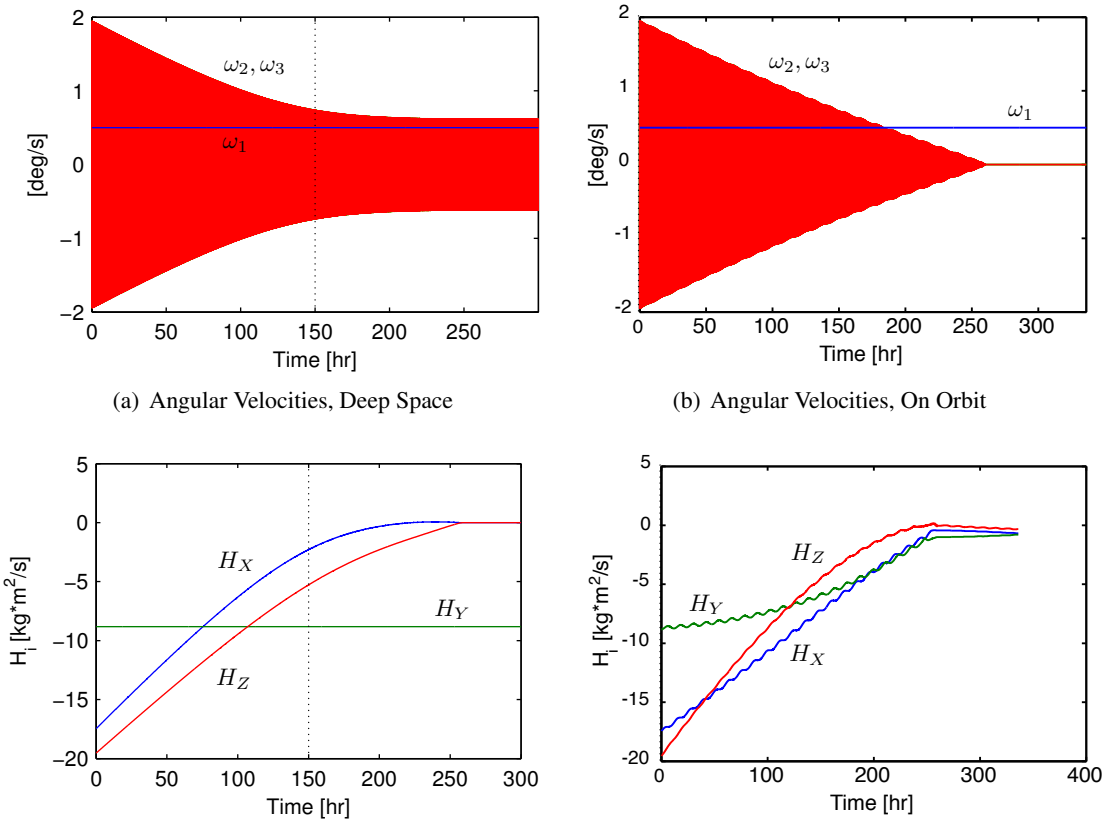

(a) Angular Velocities, Deep Space

(b) Angular Velocities, On Orbit

(c) Momentum Components H_i in servicer frame

(d) H_i in servicer frame, On Orbit

Figure 7. Angular momentum with initial conditions: $\omega = [0.5, -1.374,\ 1.374]$**,** $\Phi_0 = 30^\circ$ **comparing both deep space (left column) and on orbit (right column).**

Additional insight is gained by the inspection of the body frame angular velocities and the inertial angular momentum vector both shown in Figure 7. Clearly visible in Figure 7(a) is the constant slender axis rotation around $\hat{\boldsymbol{b}}_1$ and the convergence to angular velocity oscillation between ω_2 and ω_3 while in deep space. The steady-state angular velocities in the presented deep space case are a degenerate case of Eq. 26. The deep space case has a fixed inertial $\hat{\boldsymbol{r}}$ which provides an opportunity for the final coning motion of the debris object to satisfy the bracketed term in Eq. 26 with nonzero transverse angular velocities. Further, with the inertially fixed $\hat{\boldsymbol{r}}$ the $H_{\|_r}$ magnitude remains unaffected. Figure 7(c) shows the inertial $\boldsymbol{H}_Y$ component unchanged where the other two components are driven to zero. The combination of a coning angle and the unchanged parallel angular momentum component produces $\eta_{ss} \neq 0$ and an incomplete angular momentum reduction.

Comparison of the detumble performance reveals that the on orbit motion provides additional momentum dumping using nearly equivalent time as in deep space. The relative motion suggests greater momentum observability by the control torque leading to more effective momentum removal with greatest evidence in the angular velocity reduction in Figure 7(b). As expected, the body frame angular velocities for the on orbit case are reduced to nearly zero where the slender axis ω_1 remains unaffected. The inertial angular momentum time history in Figure 7(d) provides additional support for a more complete debris detumble. Comparision to Figure 7(c) reveals that all three inertial

momentum vectors are influence when a non-stationary $\hat{\boldsymbol{r}}$ is introduced. The adjustment during the supplementary phase does not experience an increase in angular momentum magnitude only a reconfiguration towards the $\Phi = 90^\circ$ steady-state condition. The on orbit simulation demonstrates that the inclusion of simple on orbit relative motion provides increased detumble performance further suggesting electrostatic detumble as a viable touchless detumble method.

CONCLUSIONS

Studied are the nominal push and pull equilibrium states for a cylindrical debris object in deep space. Shown is that a servicer craft can impart both a detumble torque and a nominal push or pull with a stable and predictable outcome. Developed is a generalization of the previously derived stability proof to characterize the equilibrium surfaces. The deep space projection angle dynamics and Lyapunov proof provide that nominal tugging move towards a zero projection angle where the nominal pushing move towards a 90° projection angle. The use of the 3-dimensional projection angle allows a full encapsulation of the simplified 1-dimensional rotation case.

Further studied is the detumble performance while the servicer-debris system is in a lead-follower GEO orbit around Earth. Demonstrated is a more complete detumble in comparison to the deep space case. The addition of a non-stationary inertial relative position vector provides sufficient momentum observability to effectively remove nearly all the non-slender axis momentum. Derived were the necessary conditions on the resulting angular velocities at steady state which are used to predict steady state attitude. The proposed controller is numerically verified in numerical simulation with comparisons made between deep space and on orbit performance. The presented study provides motivation for additional work regarding intelligent movement of the relative position vector for best detumble performance.

Future work will address the electrostatic detumble benefits of alternate relative orbits. It is believed that prescription of the relative motion as a control variable will greatly improve specific detumble scenarios. The steady state behavior of electrostatic detumble while on orbit will be further studied to produce more concise analytical predictions of steady state behavior.

ACKNOWLEDGMENTS

The author would like to thank the NASA Space Technology Research Fellowship (NSTRF) program, grant number NNX14AL62H, for support of this research.

REFERENCES

[1] P. Couzin, F. Teti, and R. Rembala, "Active Removal of Large Debris: System approach of deorbiting concepts and Technological issues," *6th European Conference on Space Debris*, Darmstadt, Germany, April 22–25 2013. Paper No. 6a.P-17.

[2] A. Ogilvie, J. Allport, M. Hannah, and J. Lymer, "Autonomous satellite servicing using the orbital express demonstration manipulator system," *Proc. of the 9th International Symposium on Artificial Intelligence, Robotics and Automation in Space (i-SAIRAS'08)*, 2008, pp. 25–29.

[3] W. Xu, B. Liang, B. Li, and Y. Xu, "A universal on-orbit servicing system used in the geostationary orbit," *Advances in Space Research*, Vol. 48, No. 1, 2011, pp. 95–119, 10.1016/j.asr.2011.02.012.

[4] P. Couzin, F. Teti, and R. Rembala, "Active Removal of Large Debris : Rendez-vous and Robotic Capture Issues," *2nd European Workshop on Active Debris Removal*, Paris, France, 2012. Paper #7.5.

[5] H. Schaub and D. F. Moorer, "Geosynchronous Large Debris Reorbiter: Challenges and Prospects," *The Journal of the Astronautical Sciences*, Vol. 59, No. 1–2, 2014, pp. 161–176, 10.1007/s40295-013-0011-8.

[6] D. F. Moorer and H. Schaub, "Hybrid Electrostatic Space Tug," US Patent 0036951-A1, Feb. 17 2011.

[7] D. F. Moorer and H. Schaub, "Electrostatic Spacecraft Reorbiter," US Patent 8,205,838 B2, Feb. 17 2011.

[8] H. Schaub and D. Stevenson, "Prospects Of Relative Attitude Control Using Coulomb Actuation," *Jer-Nan Juang Astrodynamics Symposium*, College Station, TX, June 25–26 2012. Paper AAS 12–607.

[9] N. Murdoch, D. Izzo, C. Bombardelli, I. Carnelli, A. Hilgers, and D. Rodgers, "Electrostatic tractor for near Earth object deflection," *59th International Astronautical Congress*, Glasgow Scotland, 2008. Paper IAC-08-A3.I.5.

[10] N. Murdoch, D. Izzo, C. Bombardelli, I. Carnelli, A. Hilgers, and D. Rodgers, "The Electrostatic Tractor for Asteroid Deflection," *58th International Astronautical Congress*, 2008. Paper IAC-08-A3.I.5.

[11] J. H. Cover, W. Knauer, and H. A. Maurer, "Lightweight Reflecting Structures Utilizing Electrostatic Inflation," US Patent 3,546,706, October 1966.

[12] D. Stevenson and H. Schaub, "Multi-Sphere Method for Modeling Electrostatic Forces and Torques," *Advances in Space Research*, Vol. 51, Jan. 2013, pp. 10–20, 10.1016/j.asr.2012.08.014.

[13] L. B. King, G. G. Parker, S. Deshmukh, and J.-H. Chong, "Spacecraft Formation-Flying using Inter-Vehicle Coulomb Forces," tech. rep., NASA/NIAC, January 2002. `http://www.niac.usra.edu`.

[14] J. Berryman and H. Schaub, "Analytical Charge Analysis for 2- and 3-Craft Coulomb Formations," *AIAA Journal of Guidance, Control, and Dynamics*, Vol. 30, Nov.–Dec. 2007, pp. 1701–1710, 10.2514/1.23785.

[15] C. R. Seubert, S. Panosian, and H. Schaub, "Tethered Coulomb Structure Applied to Close Proximity Situational Awareness," *AIAA Journal of Spacecraft and Rockets*, Vol. 49, Nov. – Dec. 2012, pp. 1183–1193, 10.2514/1.A32212.

[16] L. A. Stiles, H. Schaub, K. K. Maute, and D. F. Moorer, "Electrostatically inflated gossamer space structure voltage requirements due to orbital perturbations," *Acta Astronautica*, Vol. 84, Mar.–Apr. 2013, pp. 109–121, 10.1016/j.actaastro.2012.11.007.

[17] S. Wang and H. Schaub, "Nonlinear Charge Control for a Collinear Fixed Shape Three-Craft Equilibrium," *AIAA Journal of Guidance, Control, and Dynamics*, Vol. 34, Mar.–Apr. 2011, pp. 359–366, 10.2514/1.52117.

[18] M. A. Peck, "Prospects and Challenges for Lorentz-Augmented Orbits," *AIAA Guidance, Navigation and Control Conference*, San Francisco, CA, August 15–18 2005. Paper No. AIAA 2005-5995.

[19] B. Streetman and M. A. Peck, "New Synchronous Orbits Using the Geomagentic Lorentz Force," *AIAA Journal of Guidance, Control, and Dynamics*, Vol. 30, Nov.–Dec. 2007, pp. 1677–1690.

[20] D. Stevenson and H. Schaub, "Optimization of Sphere Population for Electrostatic Multi Sphere Model," *IEEE Transactions on Plasma Science*, Vol. 41, Dec. 2013, pp. 3526–3535, 10.1109/TPS.2013.2283716.

[21] D. Stevenson and H. Schaub, "Advances In Experimental Verification Of Remote Spacecraft Attitude Control By Coulomb Charging," *GNC 2014: 9th International ESA Conference on Guidance, Navigation and Control Systems*, Porto, Portugal, June 2–6 2014.

[22] T. Bennett and H. Schaub, "Touchless Electrostatic Three-Dimensional Detumbling of Large GEO Debris," *AAS/AIAA Spaceflight Mechanics Meeting*, Santa Fe, New Mexico, Jan. 26–30 2014. Paper AAS 14-378.

[23] E. Hogan and H. Schaub, "Relative Motion Control for Two-Spacecraft Electrostatic Orbit Corrections," *AIAA Journal of Guidance, Control, and Dynamics*, Vol. 36, Jan. – Feb. 2013, pp. 240–249, 10.2514/1.56118.

[24] E. Hogan and H. Schaub, "Space Debris Reorbiting Using Electrostatic Actuation," *AAS Guidance and Control Conference*, Breckenridge, CO, Feb. 3–8 2012. Paper AAS 12–016.

[25] U. Yamamoto and H. Yamakawa, "Two-Craft Coulomb-Force Formation Dynamics and Stability Analysis with Debye Length Characteristics," *AIAA/AAS Astrodynamics Specialist Conference and Exhibit*, Honolulu, Hawaii, Aug. 18–21 2008. Paper No. AIAA 2008-7361.

[26] M. A. Peck, B. Streetman, C. M. Saaj, and V. Lappas, "Spacecraft Formation Flying using Lorentz Forces," *Journal of British Interplanetary Society*, Vol. 60, July 2007, pp. 263–267.

[27] H. Yamakawa, M. Bando, K. Yano, and S. Tsujii, "Spacecraft Relative Dynamics under the Influence of Geomagnetic Lorentz Force," *AIAA Guidance, Navigation and Control Conference*, Toronto, Canada, Aug. 2–5 2010. Paper No. AIAA 2010-8128.

[28] W. R. Smythe, *Static and Dynamic Electricity*. McGraw–Hill, 3rd ed., 1968.

[29] J. Sliško and R. A. Brito-Orta, "On approximate formulas for the electrostatic force between two conducting spheres," *American Journal of Physics*, Vol. 66, No. 4, 1998, pp. 352–355.